2019 IEEE MTT-S International Conference on Numerical Electromagnetic and Multiphysics Modeling and Optimization (NEMO)

A New Multipactor Effect Model for Dielectric-Loaded Rectangular Waveguides

Andrés Berenguer
Dept. of Communications Engineering-I3E
Universidad Miguel Hernández de Elche
Elche, Spain
aberenguer@umh.es

Ángela Coves
Dept. of Communications Engineering-I3E
Universidad Miguel Hernández de Elche
Elche, Spain
angela.coves@umh.es

Francisco Mesa
Dept. of Applied Physics I
Universidad de Sevilla
Sevilla, Spain
mesa@us.es

Enrique Bronchalo
Dept. of Communications Engineering-I3E
Universidad Miguel Hernández de Elche
Elche, Spain
ebronchalo@umh.es

Benito Gimeno
Dept. of Applied Physics and Electromagnetism-ICMUV
Universidad de Valencia
Burjasot, Spain
benito.gimeno@uv.es

***Abstract*—Multipactor is an electron discharge that may appear in particle accelerators and microwave devices such as filters, multiplexers, and RF satellite payloads in satellite on-board equipment under vacuum conditions. When some resonance conditions are satisfied, secondary electrons get synchronized with the RF fields, and the electron population inside the device grows exponentially leading to a multipactor discharge. This multipactor discharge has some negative effects that degrade the device performance: increase of signal noise and reflected power, heating of the device walls, outgassing, detuning of resonant cavities, and even the partial or total destruction of the component. The main aim of this investigation is to show a new model for the analysis of multipactor effect in partially dielectric-loaded rectangular waveguides. For this purpose, a CAD software has been developed which allows the simulation and design of these structures out of the operation points in which this undesired multipactor effect occurs, including the main factors that drive it.**

***Index Terms*—Dielectric-loaded rectangular waveguide, electron dynamics, multipactor, secondary emision yield.**

I. Introduction

MULTIPACTOR is a high-power resonant electron discharge frequently observed in microwave and millimeterwave subsystems operating under the vacuum conditions present in a wide range of different scenarios, such as passive components of satellite communication payloads, traveling-wave tubes or particle accelerators. In an ultra-high vacuum environment, free electrons inside a microwave device are accelerated by the radio frequency (RF) electromagnetic fields, impacting against its metallic walls. If the electron impact energy is high enough, one or more secondary electrons might be released from the surface. When some resonance conditions are satisfied, secondary electrons get synchronized with the RF fields, and the electron population inside the device grows exponentially leading to a multipactor discharge.

Some works [1] take advantage of available susceptibility charts in empty parallel-plate waveguides obtained with analytical models, and they are directly used to predict multipactor breakdown in the component under study, which is going to happen in the point of highest field intensity. However, such susceptibility diagrams do not take into account important effects such as the dependence of these diagrams on elastic and inelastic electrons, as well as the 3D character of the motion of the electrons inside the waveguide, or the non-uniform nature of the electromagnetic fields in some particular cases. In addition, the multipactor effect including the presence of dielectric materials in single-surface multipactor regime has been widely investigated in the context of particle accelerators; for instance, in alumina-based dielectric-loaded accelerating structures [2], but very few contributions can be found about multipactor breakdown on dielectrics in the scenario of RF systems for space applications [3]–[5], and mostly under the parallel-plate waveguide approximation. Therefore, there is a need to accurately predict the electron discharge on devices involving partially dielectric-loaded rectangular waveguides, which are of more practical interest for satellite technology.

In Section II, the theoretical model employed for the simulations is discussed. In Section III the multipactor prediction results of an dielectric-loaded rectangular waveguide are analyzed. The susceptibility chart of it is obtained with the developed model, and the time evolution of a discharge in this waveguide is studied and discussed. Finally Section IV outlines the main conclusions of the present work.

II. Theory

Fig.1 shows the scheme of a partially dielectric-loaded rectangular waveguide of width a and height b, and whose dielectric material has relative permittivity ϵ_r. In the problem under study, the dielectric slab of thickness h and width a is placed over the bottom waveguide wall, being d the empty waveguide heigth where the effective electron travels.

978-1-5386-9516-6/19/$31.00

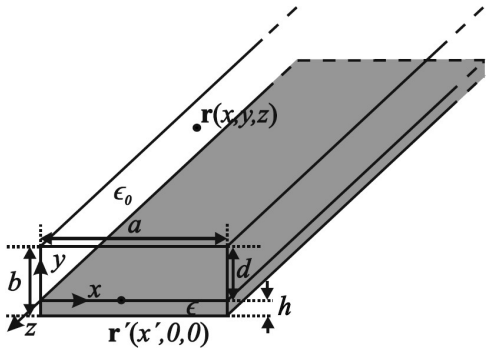

Fig. 1. Geometry of the dielectric-loaded rectangular waveguide.

A. Electron dynamics

The electron dynamics inside the waveguide is governed by the Lorentz force and related to its linear momentum,

$$\mathbf{F}_L = q(\mathbf{E} + \mathbf{v} \times \mathbf{B}) = \frac{\partial \mathbf{p}}{\partial t} \tag{1}$$

where $q = -e$ is the electron charge, $\mathbf{E}$ and $\mathbf{B} = \mu_0 \mathbf{H}$ are the total electric and magnetic fields interacting with the electron, μ_0 is the free-space magnetic permeability, and $\mathbf{v}$ is the velocity vector of the electron. The linear relativistic momentum is defined as

$$\mathbf{p} = m_0 \gamma \mathbf{v} \tag{2}$$

where m_0 is the electron rest mass, $\gamma = 1/\sqrt{1-(v/c)^2}$ the Lorentz factor, v the magnitude of the velocity vector, $c = 1/\sqrt{\mu_0 \epsilon_0}$ the speed of light in vacuum, and ϵ_0 the free-space electric permittivity. Expanding (1) and (2), the following differential equation is obtained,

$$\ddot{\mathbf{r}} = \frac{-\dot{\mathbf{r}} \times \mathbf{B} - \mathbf{E} + \dot{\mathbf{r}} \cdot (\dot{\mathbf{r}} \cdot \mathbf{E})/c^2}{A\gamma} \tag{3}$$

where $A = m_0/e$. The electron trajectory is found by numerically solving the above equations of motion. For that purpose, a velocity-Verlet algorithm [6] has been used, which assures sufficient accuracy and good efficiency provided the time step is small enough. Regarding this last point, in order to improve the accuracy and efficiency of the simulation, the following adaptive time step has been applied in the proximity of the waveguide walls, depending on the electron position,

$$\Delta t = \frac{\Delta t_0}{1 + \xi \left(\dfrac{x - a/2}{a/2} \right)^2 + \xi \left(\dfrac{y - d/2}{d/2} \right)^2} \tag{4}$$

where Δt_0 is the initial reference time step, ξ is a constant value (in this case a value of 4.0 has been chosen), and x and y are the coordinates of the electron position.

B. Electromagnetic Field, E_{RF} and H_{RF}

The RF electromagnetic field is assumed to propagate along the positive direction of the z-axis. For the sake of simplicity, the waveguide is supposed to be infinite along the z direction, and a time-harmonic dependence of the type $\exp^{i\omega t}$ is implicitly assumed, with $f = \omega/2\pi$ being the frequency and t the time measured in the laboratory reference system. The effective electron at $\mathbf{r} = (x, y, z)$ can move in the air region of height d of the rectangular waveguide. The electromagnetic fields $\mathbf{E}_{\text{RF}}$ and $\mathbf{H}_{\text{RF}}$ acting on the effective electron correspond to the modes of the partially dielectric-loaded rectangular waveguide, which are hybrid modes of TM^y and TE^y kinds [7]. We have restricted our study to the monomode regime, where only the fundamental mode, TM$^y_{10}$, propagates in the waveguide. The instantaneous field vectors interacting with the effective electron are given by

$$\mathbf{E}_{\text{RF}}(x, y, z, t) = E_0 \Re(\mathbf{e}(x, y) \exp(i(\omega t - \beta z + \varphi_0)) \tag{5a}$$

$$\mathbf{H}_{\text{RF}}(x, y, z, t) = H_0 \Re(\mathbf{h}(x, y) \exp(i(\omega t - \beta z + \varphi_0)) \tag{5b}$$

where φ_0 is the initial phase and E_0, H_0 constants related to the transmitted power in the waveguide. The modal fields $\mathbf{e}(x, y)$ and $\mathbf{h}(x, y)$ and the propagation constant β of the TM$^y_{10}$ mode can be found in [7].

C. Electrostatic Field, E_{DC}

The RF electromagnetic field will make an electron impact with any surface of the rectangular waveguide, which can result in the emission or absorption of secondary electrons. If the impacts occur on the dielectric surface, unlike the case of impacts on the metallic walls, the secondary electrons emitted by the dielectric give rise to positive charges at the impact positions on the dielectric surface, while the electrons absorbed in the dielectric layer will generate negative charges in it. These charges, which are located on the dielectric surface at positions $\mathbf{r}' = (x', 0, z')$, give rise to an electrostatic field $\mathbf{E}_{\text{DC}}$, which has to be added to the RF fields to obtain accurately the trajectory of the electrons inside the waveguide.

The electrostatic field $\mathbf{E}_{\text{DC}}$ generated by the charges on the dielectric can be obtained as,

$$\mathbf{E}_{\text{DC}}(x, y, z) = -\nabla \phi(x, y, z) \tag{6}$$

where $\phi(x, y, z)$ is the potential inside the waveguide. Using superposition, this potential due to the set of charges Q_i on the dielectric surface can be obtained by adding the individual contribution of each charge,

$$\phi(x, y, z) = \sum_i G(x - x'_i, y, |z - z'_i|) Q_i(x'_i, 0, z'_i) \tag{7}$$

where $G(x, y, z)$ is the electrostatic potential due to a unit point charge, that is, the Green's function for this problem. Due to the geometric characteristics and the linear nature of the problem under consideration it is straightforward to demonstrate, as explained in [8], that the Green's function in the spatial domain G can be obtained in the air region $y \geq 0$ as,

$$G(x, x', y, z) = \frac{2}{\epsilon_0 \pi a} \sum_{n=1}^{\infty} \sin(k_{xn} x) \sin(k_{xn} x') \times \int_0^{\infty} \frac{\sinh[k_t(d - y)] \cos(k_z z)}{k_t[\epsilon_r \coth(k_t h) + \coth(k_t d)] \sinh(k_t d)} \, dk_z \, . \tag{8}$$

In (8), if the point charge is placed at $z' \neq 0$, z must be replaced by $(z - z')$. Here it is worth noting that very efficient numerical summation and integration techniques have to be employed to compute the Green's function with sufficient accuracy and tolerable CPU times. Once the Green's function has been calculated, the $\mathbf{E}_{\mathrm{DC}}$ field is obtained by using (7) and calculating numerical differentiation of (6) by means of the central difference technique.

D. Secondary Electron Yield, SEY

The number of electrons emitted or absorbed after each impact of the effective electron on the waveguide walls is determined by the value of the Secondary Electron Yield (SEY) parameter δ ($\delta > 1$ if secondary electrons are emitted, and $\delta < 1$ if they are absorbed). The SEY is modeled by a modification of the Vaughan's model [9] that includes the effect of reflected electrons for low impact energies of primary electrons, which has to be accounted for obtaining accurate results.

In the effective electron model (EEM) assumed in this study, after the effective electron impacts at time t with any surface, $N_i(t)$ is modified according to the δ value provided by the SEY function as follows,

$$N_i(t + \Delta t) = \delta N_i(t) \tag{9}$$

where $N_i(t)$ represents the population of the ee inside the waveguide at the instant t, and Δt is the time step used in the simulations.

The secondary electron departure kinetic energy E_s after each electron impact is assumed to fit the following probability density function [10],

$$\frac{dp(E_s)}{dE_s} = C \exp\left[-\frac{\ln^2(E_s/E_m)}{2\tau^2}\right] \tag{10}$$

where C is a normalization constant, the parameter τ (typical values 0.7-0.8) determines the width of the distribution and E_m (typical values 3-4 eV) is the energy of the maximum of the spectrum. Finally, the secondary electrons after inelastic impacts are emitted following a cosine distribution of the polar angle.

III. Numerical Results and Discussion

To analyze the multipactor evolution in this waveguide, a multipactor simulation tool based on the Monte-Carlo method has been developed, including all the factors, presented in section II, driving this effect.

The susceptibility chart shown in Fig. 2 corresponds to a silver rectangular waveguide of width $a = 19.05\,\mathrm{mm}$ and height $b = 0.4\,\mathrm{mm}$, in which a thin dielectric layer (teflon) has been placed over the bottom surface of the waveguide of thickness $h = 0.025\,\mathrm{mm}$ and $\epsilon_r = 2.1$. The SEY parameters of the employed materials are given in [11].

The results of the simulations performed at the selected point $V_{\mathrm{eff}} = 672.52\,\mathrm{V}$ and $f \times d = 3.49\,\mathrm{GHz{\cdot}mm}$ are shown in Fig. 3. In this case, there is an exponential growth of the electron population (black line) that lasts approximately until

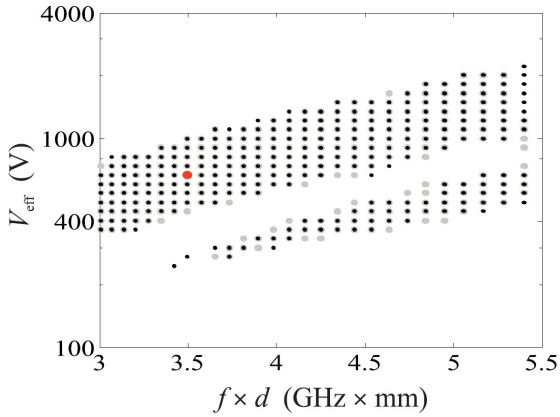

Fig. 2. Susceptibility chart of a silver rectangular waveguide partially filled with teflon (black points) with that of its equivalent empty waveguide (gray points). The point $f \times d = 3.49\,\mathrm{GHz{\cdot}mm}$ and $V_{\mathrm{eff}} = 672.52\,\mathrm{V}$ is highlighted in red.

12.5 RF cycles, associated with the emission of secondary electrons consecutively in the upper and lower walls of the waveguide, since at the selected point $\delta > 1$ on both surfaces. Then, the population, which has reached values around 10^{10} electrons, oscillates during the next 6 RF cycles, in which the appearance of a DC field in the waveguide (blue line) due to the appearance of charges on the dielectric surface (orange dots) is observed. Finally, around the 19 RF cycle, the electron population ends up being extinguished due to a low energy impacts process on the upper surface of the waveguide originated by the appearance of this DC field.

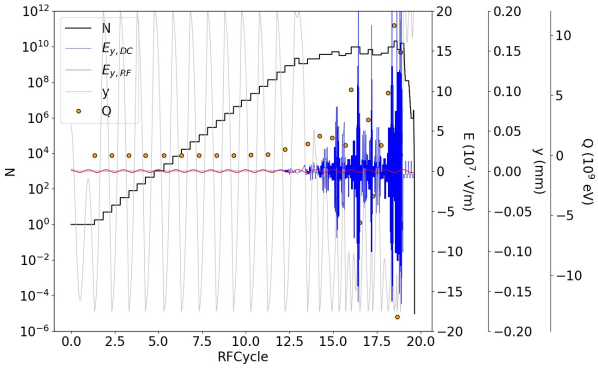

Fig. 3. Time evolution of the total number of electrons N (black line), $E_{y,\mathrm{DC}}$ at the electron position (blue line), $E_{y,\mathrm{RF}}$ (red line), electron position y (grey line) and charge Q at each inelastic impact (orange points).

In order to validate the EEM model in the partially dielectric-loaded waveguide configuration and the multipactor time-evolution shown previously, it has been demonstrated that there is no great dispersion of the electrons in the transverse direction of the waveguide during a typical simulation of an electron discharge. For this purpose, several simulations have been performed by using the developed multipactor simulator tool. In particular, a total number of 1000 effective electrons

have been launched from the center of the bottom waveguide wall, i.e. dielectric surface, considering different energies and initial angles. The arrival positions at the top wall can be fitted rather well by a 2D Gaussian distribution with $\sigma_x \simeq \sigma_z \simeq 44\mu$m. Fig. 4 shows the simulation results. Following

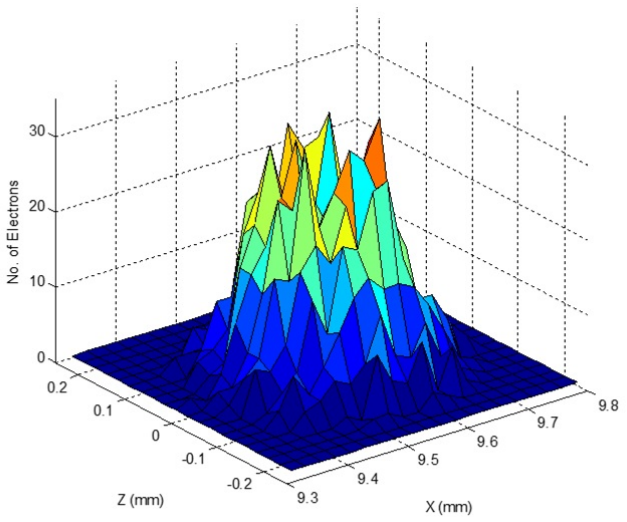

Fig. 4. Arrival positions of the effective electron at the top wall after simulating 1000 effective electrons launched from the center of the bottom dielectric surface considering random energies and initial angles.

the process of successive impacts in both walls, and assuming resonance conditions, the arrival positions distribution in the n-th impact can be easily obtained by performing a convolution of the Gaussian of the previous step with a 2D Gaussian of standard deviation of 44μm. The result is a new 2D Gaussian with $\sigma_x = \sigma_z \simeq \sqrt{n}\cdot 44\mu$m, being n the impact number. Given that at the selected first-order multipactor regime point, for each RF cycle, there are two impacts, one on each wall, then $\sigma_x = \sigma_z \simeq \sqrt{2N_{cycles}}\cdot 44\mu$m. After 12.5 RF cycles, we have a 2D Gaussian distribution of the impact positions with standard deviation $\sigma_x = \sigma_z \simeq \sqrt{2\cdot 12.5}\cdot 44\mu\text{m} = 220\mu$m. That is, after 12.5 RF cycles, when the exponential growth regime finishes due to the appearance of the DC field because of the charging of the dielectric, the diameter of the spot is about 0.5 mm. Such simulations show that the single EEM can be used for high kinetic energies of the impacting electrons, as it is the case in the multipactor resonance condition when launching the effective electron near the waveguide center, where the electric field is higher.

IV. Conclusions

A new model for multipactor effect modelling in rectangular waveguides partially filled with dielectric material has been presented. The main factors that drive this undesired effect has been analyzed rigorously. To resume, the simulations indicate that, under the conditions studied in the paper, the spread of the electron impact positions in the waveguide walls is relatively small and similar for an ensemble of individual electrons and for an effective electron accounting for all, validating the EEM model developed.

Acknowledgment

This work was supported by the Agencia Estatal de Investigación (AEI) and by the Unión Europea through the Fondo Europeo de Desarrollo Regional - FEDER - "Una manera de hacer Europa" (AEI/FEDER, UE), under the Research Projects TEC2016-75934-C4-2-R and TEC2017-84724-P.

References

[1] F. Quesada, V. Boria, B. Gimeno, D. Caete, J. Pascual, A. lvarez, J. Hueso, D. Schmitt, D. R. C. Ernst, and I. Hidalgo, "Investigation of multipactor phenomena in inductively coupled passive waveguide components for space applications," pp. 246–249, IEEE MTT-S Digest, 2006. San Francisco, CA, USA.

[2] J. Power, W. Gai, S. H. Gold, A. K. Kinkead, R. Konecny, C. Jing, W. Liu, and Z. Yusof, "Observation of multipactor in an alumina-based dielectric-loaded accelerating structure," *Physical Review Letter*, vol. 92, pp. 164801–164801, April 2004.

[3] G. Torregrosa, A. Coves, C. P. Vicente, A. M. Pérez, B. Gimeno, and V. E. Boria, "Time evolution of an electron discharge in a parallel-plate dielectric-loaded waveguide," *IEEE Electron Device Letters*, vol. 27, pp. 629–631, July 2006.

[4] A. Coves, G. Torregrosa-Penalva, C. P. Vicente, A. M. Pérez, B. Gimeno, and V. E. Boria, "Multipactor discharges in parallel-plate dielectric-loaded waveguides including space-charge effects," *IEEE Transactions on Electron Devices*, vol. 55, pp. 2505–2511, September 2008.

[5] G. Torregrosa-Penalva, A. Coves, B. Gimeno, I. Montero, C. Vicente, , and V. E. Boria, "Multipactor susceptibility charts of a parallel-plate dielectric-loaded waveguide," *IEEE Transactions on Electron Devices*, vol. 57, pp. 1160–1166, May 2010.

[6] A. Berenguer, A. Coves, E. Bronchalo, B. Gimeno, and V. E. Boria, "Analysis of multipactor effect in parallel-plate and rectangular waveguides," pp. 1564–1568, Proccedings PIERS, July 2015. Prague, Czech Republic.

[7] R. F. Harrington, *Time-Harmonic Electromagnetic Fields*. Wiley-IEEE Press, 2001.

[8] A. Berenguer, A. Coves, F. Mesa, E. Bronchalo, B. Gimeno, , and V. E. Boria, "Calculation of the electrostatic field in a dielectric-loaded waveguide due to an arbitrary charge distribution on the dielectric layer," pp. 3251–3255, Proccedings PIERS, August 2016. Shanghai, China.

[9] R. Vaughan, "A new formula for secondary emission yield," *IEEE Transactions on Electron Devices*, vol. 36, pp. 1963–1989, 1989.

[10] J. J. Scholtz, D. Dijkkamp, and R. Schmitz, "Secondary electron emission properties," *Philips J. Res*, vol. 50, pp. 375–389, 1996.

[11] A. Berenguer, A. Coves, F. Mesa, E. Bronchalo, and B.Gimeno, "Analysis of multipactor effect in a partially dielectric-loaded rectangular waveguide," *IEEE Transactions on Plasma Science*, vol. 47, no. 1, pp. 259–265, 2019.